

Quasi-Bell states in a strongly coupled qubit-oscillator system and their delocalization in the phase space

R. Chakrabarti and B. Virgin Jenisha

*Department of Theoretical Physics, University of Madras,
Maraimalai Campus, Guindy, Chennai 600 025, India*

Abstract

We study the evolution of bipartite entangled quasi-Bell states in a strongly coupled qubit-oscillator system in the presence of a static bias, and extend it to the ultra-strong coupling regime. Using the adiabatic approximation the reduced density matrix of the qubit is obtained for the strong coupling domain in *closed form* that involves linear combinations of the Jacobi theta functions. The reduced density matrix of the oscillator yields the phase space Husimi Q -distribution. In the strong coupling regime the Q -function evolves to uniformly separated macroscopically distinct Gaussian peaks representing 'kitten' states at certain specified times that depend on *multiple* time scales present in the interacting system. For the ultra-strong coupling realm the delocalization in the phase space of the oscillator is studied by using the Wehrl entropy and the complexity of the quantum state. For a small phase space amplitude the entangled quasi-Bell state develops, during its time evolution, squeezing property and nonclassicality of the photon statistics which are measured by the quadrature variance and the Mandel parameter, respectively.

I Introduction

One of the ubiquitous and most important models in the quantum physics describes a two-level system (qubit) interacting with a simple harmonic oscillator. In quantum optics it describes the interaction of an atom with an electromagnetic field mode in a cavity. For a small detuning between the oscillator and the qubit frequencies, and also for a weak qubit-oscillator coupling, the dynamical behavior of the interacting system is accurately described by the exactly solvable Jaynes-Cummings model [1] that employs the rotating wave approximation. Recently, however, a variety of experimental situations pertaining to the stronger coupling domain, where the rotating wave approximation no longer holds, have been investigated. Various experimental realizations such as a nanomechanical resonator capacitively coupled to a Cooper-pair box [2], a quantum semiconductor microcavity undergoing excitonic transitions [3], a flux-biased superconducting quantum circuit that uses large nonlinear inductance of the Josephson junctions to achieve ultrastrong coupling with a coplanar waveguide resonator [4] have been achieved. The superconducting circuits based on the Josephson junctions behave, in certain parametric range, as effective two level systems, and can exhibit macroscopic quantum coherence [5, 6]. These artificial atoms have advantage in that they offer additional flexibility in selecting the control parameters which facilitate experimental tests of fundamental quantum mechanical principles at a macroscopic scale [7]. The tailor-made physical characteristics of the superconducting circuits and their easy adjustability, say by changing external magnetic fields, make them particularly suitable candidates for the quantum simulators [8-10]. Integrated hybrid quantum circuits involving atoms, spins, cavity photons, and superconducting qubits with nanomechanical resonators are also of much interest [11].

Moving beyond the rotating wave approximation in these strongly interacting systems one needs to incorporate terms in the qubit-oscillator interaction Hamiltonian that do not preserve the total excitation number. In the parametric regime where the oscillator frequency dominates the qubit frequency the authors of Refs. [12, 13] have advanced an adiabatic approximation scheme that utilizes the disparity of the time scales of the qubit and the oscillator. The dynamical state of the fast-moving oscillator is assumed to instantaneously adjust to the slow-changing state of the qubit. This facilitates decoupling of the full Hamiltonian into sectors related to each time scale, and allows approximate evaluation [12] of eigenstates of the system. In addition, an analytical expression of the time-dependent behavior of the two level system has been obtained [12] in a relatively weak coupling limit. Studying a system of two qubits coupled to a single oscillator mode in the context of the Tavis-Cummings model the authors of Ref. [14] have analytically evaluated the collapse and revival dynamics of the qubit reduced density matrix elements. Their procedure employs the Poisson sum formula [15] that leads to expressions of the said elements as infinite sums. Following the extensive experimental developments [5, 6] for the superconducting qubits, a static bias term has been included in the qubit Hamiltonian and the corresponding energy spectrum has been investigated [13, 16]. A time-dependent bias acting as a control parameter has also been considered [17].

For the coupled qubit-oscillator system the entangled quasi-Bell states are found to be of much interest. Usually known as the Schrödinger cat states they exhibit entanglement of the microscopic atomic states and the photonic coherent states that can be regarded as macroscopic for reasonably large values of the coherent state amplitudes. In the context of quantum information theory the hybrid entanglement involving a discrete and a continuous quantum variable may offer advantages such as achieving near-deterministic quantum teleportation [18]. Moreover, hybrid entanglement lies at the heart of the elegant quantum bus [19] approach where direct qubit-qubit interactions are avoided since a common continuous mode plays the mediating role. The Bell inequality tests involving these qubit-field entangled states have been proposed [20] recently. Realization of the micro-macro entangled states via a controllable interaction of a single-mode microwave cavity field with a superconducting charge qubit, and the subsequent creation of the superposition of macroscopically distinguishable field modes by virtue of measuring the charge states of the qubit have been proposed [21]. Much experimental

activity [22] is currently aimed at demonstrating such hybrid entanglement. Generation of the optical hybrid entanglement by the quantum superposition of non-Gaussian operations on distinct modes has been achieved [23]. Also following a measurement based approach, the hybrid entanglement between two remote nodes living in the Hilbert spaces of different dimensionality has been established [24]. The superconducting circuits have also been used for controllable and deterministic generation of complex superposition of states [25-28].

Our objective in the present work is twofold. Within the adiabatic approximation scheme we analytically study the time dependence of quasi-Bell states in a coupled qubit-oscillator system endowed with a dominant oscillator frequency and an external static bias of the qubit. Our study includes both the strong and the ultra-strong coupling domains. Starting with a quasi-Bell bipartite initial state we obtain the evolution of the reduced density matrices of the qubit and the oscillator, respectively. The qubit density matrix provides the von Neumann entropy of the system that measures the entanglement and the mixedness of the state. Proceeding further, the oscillator reduced density matrix that yields the Husimi Q -function [29] on the phase space is studied. In the strong coupling regime we retain up to the quadratic terms in the Laguerre polynomials in the phase factors and analytically express the reduced density matrix elements in closed forms via the Jacobi theta functions. To evaluate the analytical expressions we treat the bias perturbatively, and retain terms up to second order in the expansion parameter. The summation procedure may, however, be extended to an arbitrary order. The Q -distribution provides the variance of the quadrature variables of the oscillator as linear combinations of the Jacobi theta functions. We will later specify the parametric range where our theta function based construction is valid. In its region of validity the leading terms in the theta function structure provides simple estimates, say, for the revival time for the off-diagonal qubit matrix element. Analysing the Q -function in the Kerr-like nonlinear self-interacting photonic models it has been observed [30-33] that an initial coherent state therein evolves, at certain specified times, to macroscopic superposition of coherent states popularly known as ‘kitten’ states. In the current qubit-oscillator interacting model the reduced density matrix of the oscillator shows similar properties with, however, an important distinction that stems from the existence of interaction-generated multiple time scales.

In the ultra-strong coupling regime we employ the long range time dependence of the Wehrl entropy [34] and the complexity [35] of the Q -distribution that measure the delocalization of the oscillator on the phase space. An analytical evaluation of the complexity of the coupled qubit-oscillator system is developed. Both of these measures of delocalization are found to be qualitatively similar. The time dependence of the Wehrl entropy in the ultra-strong coupling domain exhibits, after a transient period of rapid build up, a quasi-stationary behavior modulo the random high frequency fluctuations. We estimate the initial production-time of the Wehrl entropy. For small values of the amplitude of the quasi-Bell state on the phase space, interference of modes produces the squeezing effect. Using the Mandel parameter [36] the nonclassicality of the photon statistics is also observed in this instance.

II The reduced density matrices

We study a coupled qubit-oscillator system with the Hamiltonian [12, 13] that reads in natural units ($\hbar = 1$) as follows:

$$H = -\frac{\Delta}{2}\sigma_x - \frac{\epsilon}{2}\sigma_z + \omega a^\dagger a + \lambda\sigma_z(a^\dagger + a), \quad (2.1)$$

where the harmonic oscillator with a frequency ω is described by the raising and lowering operators ($a^\dagger, a|\hat{n} \equiv a^\dagger a$), and the qubit characterized by an energy splitting Δ as well as an external static bias ϵ is expressed via the spin variables (σ_x, σ_z). The qubit-oscillator coupling strength is denoted by λ . The Fock states $\{\hat{n}|n\rangle = n|n\rangle, n = 0, 1, \dots; a|n\rangle = \sqrt{n}|n-1\rangle, a^\dagger|n\rangle = \sqrt{n+1}|n+1\rangle\}$ provide the basis for the oscillator, and the eigenstates $\sigma_z|\pm 1\rangle = \pm|\pm 1\rangle$ span the space of the qubit. The Hamiltonian (2.1) is not known to be exactly solvable. In the present work we follow the adiabatic

approximation [12, 13] that hinges on the separation of the time scales governed by the high oscillator frequency and the (renormalized) low qubit frequency: $\omega \gg \Delta$.

To facilitate our construction of the evolution of the quasi-Bell states, we, following [12], now give a short review of the diagonalization process of the Hamiltonian (2.1) in the adiabatic approximation scheme. The high-frequency oscillator is assumed to instantaneously adjust to the slow-changing state of the qubit observable σ_z so that the construction permits, in the course of diagonalization of the oscillator mode, replacing the spin-variable σ_z with its eigenvalue: ± 1 . The effective Hamiltonian of the harmonic oscillator now reads

$$H_{\mathcal{O}} = \omega a^\dagger a \pm \lambda(a^\dagger + a). \quad (2.2)$$

The number states which are shifted symmetrically by the displacement operator diagonalize the above Hamiltonian:

$$|n_\pm\rangle = D^\dagger(\pm\lambda/\omega)|n\rangle, \quad D(\alpha) = \exp(\alpha a^\dagger - \alpha^* a), \quad (2.3)$$

where the degenerate eigenenergies are as follows:

$$E_n^\pm \equiv \mathcal{E}_n = n\omega - \frac{\lambda^2}{\omega}. \quad (2.4)$$

Identically displaced states maintain orthonormality: $\langle m_\pm | n_\pm \rangle = \delta_{m,n}$, whereas the overlap between the Fock states displaced in opposite directions is given by [12]

$$\langle m_- | n_+ \rangle = \begin{cases} (-1)^{m-n} \exp\left(-\frac{x}{2}\right) x^{\frac{m-n}{2}} \sqrt{n!/m!} L_n^{m-n}(x) & \forall m \geq n, \\ \exp\left(-\frac{x}{2}\right) x^{\frac{n-m}{2}} \sqrt{m!/n!} L_m^{n-m}(x) & \forall m < n. \end{cases} \quad (2.5)$$

In (2.5) the associated Laguerre polynomial reads $L_n^j(x) = \sum_{k=0}^n (-1)^k \binom{n+j}{n-k} \frac{x^k}{k!}$, and the parameter $x = (2\lambda/\omega)^2$ acts as the perturbative expansion parameter.

After diagonalizing the high frequency oscillator component of the Hamiltonian, one now turns attention to the low frequency qubit part. Tensoring the qubit states with the displaced oscillator basis states $\{|\pm 1, n_\pm\rangle | \forall n = 0, 1, \dots\}$ the corresponding matrix elements of the Hamiltonian may now be readily constructed. For a dominant oscillator frequency $\Delta/\omega \ll 1$ one may neglect [12] the matrix elements that mix the oscillator states with different eigenvalues of its number operator. This reduces the Hamiltonian to a block-diagonal form where each block mixes the displaced oscillator states with identical number of photons. The Hamiltonian for the n -th block assumes the form:

$$H = \begin{pmatrix} n\omega - \frac{\lambda^2}{\omega} - \tilde{\epsilon} & \delta_n \\ \delta_n & n\omega - \frac{\lambda^2}{\omega} + \tilde{\epsilon} \end{pmatrix}, \quad \delta_n = -\frac{\tilde{\Delta}}{2} L_n(x), \quad \tilde{\Delta} = \Delta \exp\left(-\frac{x}{2}\right), \quad \tilde{\epsilon} = \frac{\epsilon}{2} \quad (2.6)$$

that may be diagonalized in the basis of the eigenstates listed below

$$|\mathcal{E}_n^\pm\rangle = \sqrt{\frac{\chi_n \mp \tilde{\epsilon}}{2\chi_n}} |1, n_+\rangle \pm \frac{\delta_n}{|\delta_n|} \sqrt{\frac{\chi_n \pm \tilde{\epsilon}}{2\chi_n}} |-1, n_-\rangle, \quad (2.7)$$

where the respective eigenvalues read

$$\mathcal{E}_n^\pm = n\omega - \lambda^2/\omega \pm \chi_n, \quad \chi_n = \sqrt{\delta_n^2 + \tilde{\epsilon}^2}. \quad (2.8)$$

Given the above construction of the eigenstates of the system we now study the time evolution of the qubit-oscillator entanglement in the presence of a bias ($\epsilon \neq 0$). The quasi-Bell initial states of the coupled system read

$$|\psi(0)\rangle^{(\pm)} = \frac{1}{\sqrt{2}} (|1, \alpha\rangle \pm |-1, -\alpha\rangle), \quad |\alpha\rangle = D(\alpha)|0\rangle, \quad (2.9)$$

where the coherent state $\{|\alpha\rangle \forall \alpha = \text{Re}(\alpha) + i \text{Im}(\alpha) \in \mathbb{C}\}$ for the oscillator degree of freedom is realized by the action of the displacement operator on the vacuum. The evolution of the initial state (2.9) is given by

$$|\psi(t)\rangle^{(\pm)} = \frac{1}{\sqrt{2}} \exp\left(-\frac{1}{2}|\alpha_+|^2 - i\left(\text{Im}(\alpha)\frac{\lambda}{\omega} + \mathcal{E}_n t\right)\right) \times \\ \times \sum_{n=0}^{\infty} \frac{1}{\sqrt{n!}} \alpha_+^n \left[\Xi_n^{\pm} \exp(-i\chi_n t) |\mathcal{E}_n^+\rangle \mp (-1)^n \frac{\delta_n}{|\delta_n|} \Xi_n^{\mp} \exp(i\chi_n t) |\mathcal{E}_n^-\rangle \right], \quad (2.10)$$

where $\alpha_+ = \alpha + \lambda/\omega$, and $\Xi_n^{\pm} = \sqrt{\frac{\chi_n - \tilde{\epsilon}}{2\chi_n}} \pm (-1)^n \frac{\delta_n}{|\delta_n|} \sqrt{\frac{\chi_n + \tilde{\epsilon}}{2\chi_n}}$. On the rhs of (2.10) and hereafter the upper and the lower signs refer to respective quasi-Bell states given in (2.9). The construction of the state (2.10) readily yields the evolution of the density matrix of the composite bipartite system:

$$\rho^{(\pm)}(t) = |\psi(t)\rangle^{(\pm)} \langle \psi(t)|. \quad (2.11)$$

The marginalized density matrices for the individual degrees of freedom may be obtained by partial tracing of the composite density matrix (2.11). For instance, tracing of the oscillator degree of freedom yields the reduced density matrix of the qubit. Its explicit structure obtained via (2.11, 2.10) assumes the form

$$\rho_{\mathcal{Q}}^{(\pm)}(t) \equiv \text{Tr}_{\mathcal{O}} \rho^{(\pm)}(t) = \begin{pmatrix} \frac{1}{2} \mp \zeta & \pm \xi^{(\pm)} \\ \pm (\xi^{(\pm)})^* & \frac{1}{2} \pm \zeta \end{pmatrix}, \quad (2.12)$$

where the components read

$$\zeta = \tilde{\epsilon} \exp(-|\alpha_+|^2) \sum_{n=0}^{\infty} (-1)^n \frac{|\alpha_+|^{2n}}{n!} \delta_n \frac{\sin^2 \chi_n t}{\chi_n^2}, \quad (2.13)$$

$$\xi^{(\pm)} = \frac{1}{2} \exp(-|\alpha_+|^2) \sum_{n,m=0}^{\infty} (-1)^m \frac{(\alpha_+)^n (\alpha_+^*)^m}{\sqrt{n! m!}} C_n^{\pm}(t) C_m^{\mp}(t) \times \\ \times \exp(-i(n-m)\omega t) \langle m_- | n_+ \rangle, \quad (2.14)$$

and the coefficients are given by

$$C_n^{\pm}(t) = A_n^{\mp} \exp(i\chi_n t) + B_n^{\pm} \exp(-i\chi_n t), \quad (2.15)$$

$$A_n^{\pm} = \frac{\chi_n + \tilde{\epsilon} \pm (-1)^n \delta_n}{2\chi_n}, \quad B_n^{\pm} = \frac{\chi_n - \tilde{\epsilon} \pm (-1)^n \delta_n}{2\chi_n}. \quad (2.16)$$

It follows from (2.13) that in the bias-free limit ($\epsilon = 0$) the diagonal elements of the reduced density matrix (2.12) of the qubit are time-independent. In the said limit it follows

$$C_n^{\pm}(t)|_{\epsilon=0} = \cos \delta_n t \mp i(-1)^n \sin \delta_n t = \exp(\mp i(-1)^n \delta_n t). \quad (2.17)$$

In general, the pair of eigenvalues of the qubit density matrix (2.12)

$$\frac{1}{2} + \varpi^{(\pm)}, \quad \frac{1}{2} - \varpi^{(\pm)}, \quad \varpi^{(\pm)} = \sqrt{\zeta^2 + |\xi^{(\pm)}|^2} \quad (2.18)$$

allows us to compute its von Neumann entropy $S(\rho_{\mathcal{Q}}) \equiv -\text{Tr}(\rho_{\mathcal{Q}} \log \rho_{\mathcal{Q}})$ as

$$S_{\mathcal{Q}}^{(\pm)} = -\left(\frac{1}{2} + \varpi^{(\pm)}\right) \log\left(\frac{1}{2} + \varpi^{(\pm)}\right) - \left(\frac{1}{2} - \varpi^{(\pm)}\right) \log\left(\frac{1}{2} - \varpi^{(\pm)}\right). \quad (2.19)$$

Similarly the trace over the qubit basis produces the reduced density matrix of the oscillator:

$$\rho_{\mathcal{O}}^{(\pm)}(t) \equiv \text{Tr}_{\mathcal{Q}} \rho^{(\pm)}(t) \quad (2.20)$$

that may be expressed, via (2.10), in terms of the displaced number states as follows:

$$\begin{aligned} \rho_{\mathcal{O}}^{(\pm)}(t) = & \frac{1}{2} \exp(-|\alpha_+|^2) \sum_{n,m=0}^{\infty} \frac{(\alpha_+)^n (\alpha_+^*)^m}{\sqrt{n!m!}} \left(\mathbf{C}_n^{\pm}(t) \mathbf{C}_m^{\pm}(t)^* |n_+\rangle\langle m_+| \right. \\ & \left. + (-1)^{n+m} \mathbf{C}_n^{\mp}(t)^* \mathbf{C}_m^{\mp}(t) |n_-\rangle\langle m_-| \right) \exp(-i(n-m)\omega t). \end{aligned} \quad (2.21)$$

Apart from employing the adiabatic approximation *no other* simplification has been made for deriving the reduced density matrix elements (2.13, 2.14, 2.21), which will later serve as benchmarks for checking the accuracy of the corresponding closed form evaluations.

To obtain measures of the entanglement and the mixedness of the bipartite system the von Neumann entropy of the reduced density matrix of the qubit may be considered. It is well-known [37] that if a composite system, comprising of two subsystems, resides in a pure state, the entropies of both subsystems are equal. In the present example it holds for the oscillator with an infinite dimensional Hilbert space and the two-level qubit interacting with it: $S_{\mathcal{Q}}^{(\pm)} = S_{\mathcal{O}}^{(\pm)} \equiv S^{(\pm)}$.

III The qubit density matrix

We now focus towards obtaining a closed form analytical evaluation of the qubit density matrix in the parametric regime where the oscillator frequency sets the dominant scale and the following hierarchy is maintained: $\epsilon < \Delta < \omega$. In the perturbative expansion given below we retain up to the second order terms in the bias parameter: $O(\epsilon^2)$. The higher order terms in ϵ may, however, be systematically taken into account in our perturbative scheme. Furthermore, in the following evaluation, we investigate the first few collapses and revivals of the density matrix elements. Consequently, for the purpose of simplicity, we neglect ϵ dependent terms in phases as they will be important only in the long time limit. Previous attempts in analytical evaluation of the elements of the density matrices include Refs. [12, 14]. Reflecting the weak coupling limit $\lambda \ll \omega$, the summation technique adopted in [12] retains terms $O(x) \sim O((\lambda/\omega)^2)$. For analytically evaluating the density matrix elements in the context of the Tavis-Cummings model at higher values of the qubit-oscillator coupling strength the authors of Ref. [14] have developed a method based on the Poisson sum formula. They have retained contributions up to the quadratic terms in the expansion of the Laguerre polynomials: $L_n(x) = 1 - nx + \frac{1}{2!} \binom{n}{2} x^2 + O(x^3)$.

We now provide an alternate method of summing the series in (2.13, 2.14) by employing the Jacobi theta functions. This method has an additional benefit in that it expresses the matrix elements in a closed form. The series expansions of the Jacobi theta functions [15] relevant in our case depend on two complex arguments (q, z) :

$$\vartheta_3(q, z) = \sum_{n=-\infty}^{\infty} q^{n^2} \exp(2inz), \quad \vartheta_4(q, z) = \sum_{n=-\infty}^{\infty} (-1)^n q^{n^2} \exp(2inz). \quad (3.1)$$

The series sums in (3.1) are convergent for the choice $\text{Re}(q) < 1$. In our summation scheme we retain contributions $O(x^2)$ in the density matrix elements and consider up to quadratic terms in the Laguerre polynomials. To proceed, we, following [14], approximate at a suitably large value of $|\alpha_+|^2$ the Poisson distribution in (2.13, 2.14) with the corresponding Gaussian limit:

$$P(n) \equiv \exp(-|\alpha_+|^2) \frac{|\alpha_+|^{2n}}{n!} \rightarrow \frac{1}{\sqrt{2\pi|\alpha_+|^2}} \exp\left(-\frac{(n-|\alpha_+|^2)^2}{2|\alpha_+|^2}\right). \quad (3.2)$$

For a large value of $|\alpha_+|^2$ the lower limit of the series in (2.13, 2.14) may be extended to $(-\infty)$. Due to the sharp decay of the Gaussian function for the parametric regime considered here the error encountered is quite small. This process is similar to the evaluation [14] of Fourier components via the Gaussian integration technique in the Poisson-sum method, where the lower limit of integration is extended to $(-\infty)$. We note that a truncated series at the lower limit in the sum (3.1) *remains convergent* in the domain $\text{Re}(q) < 1$, and it may be viewed as a close analog of the theta function. Since the difference between these alternate cases in our parametric regime is quite small we retain the standard definition (3.1). The resultant closed form expressions for the elements of the density matrix (2.12) are now given by

$$\zeta = -\frac{\epsilon}{2\tilde{\Delta}} \left[\exp\left(-2|\alpha_+|^2\right) \left(1 - f(1+x) + \frac{3}{4}f^2\right) - \frac{\exp\left(-|\alpha_+|^2/2\right)}{\sqrt{2\pi|\alpha_+|^2}} \text{Re}\{\Theta(\tau)\} \right], \quad (3.3)$$

$$\begin{aligned} \xi^{(\pm)} = & \frac{1}{2} \left(1 + f + \frac{f^2}{4}\right) \exp\left(-2|\alpha_+|^2 - \frac{x}{2}\right) + \frac{\epsilon}{\tilde{\Delta}} \zeta + \frac{\exp\left(-(x + |\alpha_+|^2)/2\right)}{\sqrt{2\pi|\alpha_+|^2}} \left(x^{\frac{1}{2}} \mathcal{R}_1 \times \right. \\ & \times \text{Re} \left[\varphi_{1,0} \vartheta_4(q, z_1) + \frac{f}{2} \varphi_{3,1} \vartheta_4(q, z_3) \right] + \frac{x}{2} \mathcal{R}_2 \text{Re} \left[\left(\tilde{\varphi}_1 + \frac{f}{3} \tilde{\varphi}_3 \right) \vartheta_4(\mathbf{q}, \mathfrak{z}_2) \right] \\ & + \frac{x^{\frac{3}{2}}}{6} \mathcal{R}_3 \text{Re}[\varphi_{3,3} \vartheta_4(q, z_3)] + \frac{x^2}{24} \mathcal{R}_4 \text{Re}[\tilde{\varphi}_3^2 \vartheta_4(\mathbf{q}, \mathfrak{z}_4)] - i \frac{\epsilon}{2\tilde{\Delta}} \text{Im}[\varphi_{0,0} \vartheta_4(q, z_0)] \\ & + \frac{\epsilon^2}{\tilde{\Delta}^2} \left[x \mathcal{R}_2 \text{Re} \left[\left(\frac{1}{2} + x \right) \varphi_{2,2} \vartheta_4(q, z_2) - \frac{5f}{6} \varphi_{4,3} \vartheta_4(q, z_4) - \left(\frac{1}{2} + x \right) \tilde{\varphi}_1 \right. \right. \\ & \left. \left. - \frac{5f}{6} \tilde{\varphi}_3 \right) \vartheta_4(\mathbf{q}, \mathfrak{z}_2) \right] + \frac{x^2}{24} \mathcal{R}_4 \text{Re}[\varphi_{4,6} \vartheta_4(q, z_4) - \tilde{\varphi}_3^2 \vartheta_4(\mathbf{q}, \mathfrak{z}_4)] \right] \pm i \frac{\epsilon}{\tilde{\Delta}} \left[x^{\frac{1}{2}} \mathcal{I}_1 \times \right. \\ & \times \text{Re} \left[\left(1 + \frac{x}{2}\right) \varphi_{1,0} \vartheta_3(q, z_1) + \frac{f}{2} \varphi_{3,1} \vartheta_3(q, z_3) - \left(\left(1 + \frac{x}{2}\right) \tilde{\varphi}_0^{\frac{1}{2}} + \frac{f}{2} \tilde{\varphi}_2^{\frac{1}{2}} \right) \times \right. \\ & \left. \left. \times \vartheta_3(\mathbf{q}, \mathfrak{z}_1) \right] + \frac{x^2}{2} \mathcal{I}_2 \text{Re}[\varphi_{2,2} \vartheta_3(q, z_2) - \tilde{\varphi}_1 \vartheta_3(\mathbf{q}, \mathfrak{z}_2)] + \frac{x^{\frac{3}{2}}}{6} \mathcal{I}_3 \text{Re}[\varphi_{3,3} \vartheta_3(q, z_3) \right. \\ & \left. - \tilde{\varphi}_1^{\frac{3}{2}} \vartheta_3(\mathbf{q}, \mathfrak{z}_3)] \right] - i \frac{\epsilon}{\tilde{\Delta}} \left[x^{\frac{1}{2}} \mathcal{R}_1 \text{Im} \left[\left(1 + \frac{x}{2}\right) \varphi_{1,0} \vartheta_4(q, z_1) - \frac{f}{2} \varphi_{3,1} \vartheta_4(q, z_3) \right. \right. \\ & \left. \left. + \frac{x}{2} \tilde{\varphi}_0^{\frac{1}{2}} \vartheta_4(\mathbf{q}, \mathfrak{z}_1) \right] + x \mathcal{R}_2 \text{Im} \left[\frac{1}{2} (1+x) \varphi_{2,2} \vartheta_4(q, z_2) - \frac{f}{3} \varphi_{4,3} \vartheta_4(q, z_4) \right. \right. \\ & \left. \left. + \frac{x}{2} \tilde{\varphi}_1 \vartheta_4(\mathbf{q}, \mathfrak{z}_2) \right] + \frac{x^{\frac{3}{2}}}{6} \mathcal{R}_3 \text{Im}[\varphi_{3,3} \vartheta_4(q, z_3)] + \frac{x^2}{24} \mathcal{R}_4 \text{Im}[\varphi_{4,6} \vartheta_4(q, z_4)] \right] \\ & \mp \left[x^{\frac{1}{2}} \mathcal{I}_1 \text{Im} \left[\varphi_{1,0} \vartheta_3(q, z_1) - \frac{f}{2} \varphi_{3,1} \vartheta_3(q, z_3) \right] - \frac{x}{2} \mathcal{I}_2 \text{Im} \left[\left(\tilde{\varphi}_1 - \frac{f}{3} \tilde{\varphi}_3 \right) \vartheta_3(\mathbf{q}, \mathfrak{z}_2) \right] \right. \\ & \left. + \frac{x^{\frac{3}{2}}}{6} \mathcal{I}_3 \text{Im}[\varphi_{3,3} \vartheta_3(q, z_3)] - \frac{x^2}{24} \mathcal{I}_4 \text{Im} \left[\tilde{\varphi}_3^2 \vartheta_3(\mathbf{q}, \mathfrak{z}_4) \right] \right] \\ & \pm \frac{2\tilde{\epsilon}^2}{\tilde{\Delta}^2} \left[x^{\frac{1}{2}} \mathcal{I}_1 \text{Im} \left[(1+x) \varphi_{1,0} \vartheta_3(q, z_1) + \frac{3f}{2} \varphi_{3,1} \vartheta_3(q, z_3) - x \tilde{\varphi}_0^{\frac{1}{2}} \vartheta_3(\mathbf{q}, \mathfrak{z}_1) \right] \right. \\ & \left. - x \mathcal{I}_2 \text{Im} \left[x \varphi_{2,2} \vartheta_3(q, z_2) - \left(\left(\frac{1}{2} + x \right) \tilde{\varphi}_1 + \frac{5f}{6} \tilde{\varphi}_3 \right) \vartheta_3(\mathbf{q}, \mathfrak{z}_2) \right] \right. \\ & \left. + \frac{x^{\frac{3}{2}}}{6} \mathcal{I}_3 \text{Im} \left[\varphi_{3,3} \vartheta_3(q, z_3) \right] - \frac{x^2}{24} \mathcal{I}_4 \text{Im} \left[\tilde{\varphi}_3^2 \vartheta_3(\mathbf{q}, \mathfrak{z}_4) \right] \right], \quad (3.4) \end{aligned}$$

where the parameters and phases given above read as follows: $f = x|\alpha_+|^2$, $\tau = \tilde{\Delta} t$, $q(\tau) = \exp\left(-\frac{1}{2|\alpha_+|^2} - i\frac{x^2\tau}{4}\right)$, $\mathbf{q} = \exp\left(-\frac{1}{2|\alpha_+|^2}\right)$, $z_j(\tau) = \frac{1}{2}(x(1 + (1-j)\frac{x}{4})\tau - i)$, $\mathfrak{z}_j(\tau) = -\frac{1}{2}(j\frac{x^2}{4}\tau + i)$, $\varphi_{j,\ell}(\tau) = \exp\left(-i\tau\left(1 - j\frac{x}{2} + \ell\frac{x^2}{4}\right)\right)$, $\tilde{\varphi}_j(\tau) = \exp(i\tau x(1 - j\frac{x}{4}))$, $\mathcal{R}_n = \text{Re}(\tilde{\alpha}^{(n)})$, $\mathcal{I}_n = \text{Im}(\tilde{\alpha}^{(n)})$,

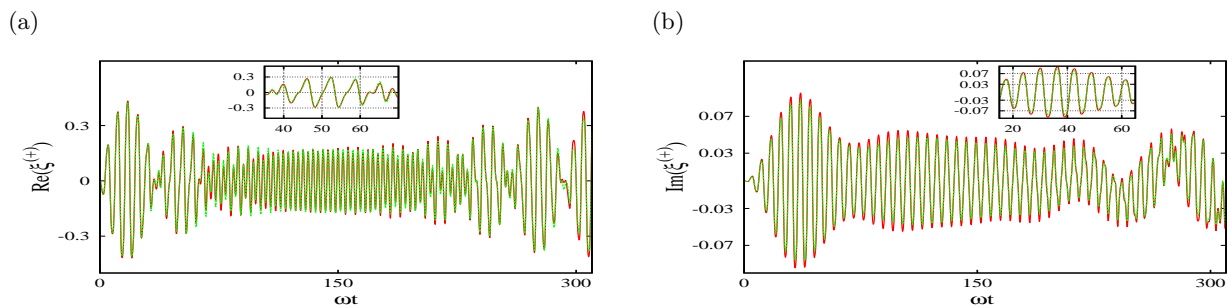


Figure 1: The evaluation of the (a) real and (b) imaginary parts of the off-diagonal component $\xi^{(+)}$ of the density matrix for the values $\lambda = 0.15\omega$, $\Delta = 0.15\omega$, $\epsilon = 0.01\omega$ and $\alpha = 2$ using the series (2.14) (red solid) that provides exact result *within the adiabatic scheme*, and the theta function (3.4) (green dashed) based result. In this instance and hereafter we study evolution w.r.t. the *scaled time* ωt .

$\tilde{\alpha}^{(n)} = \alpha_+^n e^{-in\omega t}$. The linear combination of theta functions used in (3.4) is given by $\Theta(\tau) = \varphi_{0,0}\vartheta_4(q, z_0) - f(1+x)\varphi_{2,0}\vartheta_4(q, z_2) + \frac{3}{4}f^2\varphi_{4,2}\vartheta_4(q, z_4)$. This completes our closed form evaluation of the elements of the reduced density matrix of the qubit via the Jacobi theta functions. For moderately large coupling ($\lambda/\omega \lesssim 0.20$) this summation technique agrees well with the series evaluations based on (2.13, 2.14). Concerning our choice of the bias parameter we note that as we have included terms up to $O(\epsilon^2)$, we need to maintain the order of the dimensionless ratio $\epsilon/\tilde{\Delta} \sim 0.1$. As the norm $|\alpha_+|$ appears in the coefficients of the perturbative terms as well as in the Gaussian factors, we choose it in the optimum range $|\alpha_+| \sim 1.5 - 2$. These restrictions describe the parametric regime in which our theta functions based analytical evaluations hold. The fluctuation ζ of the diagonal qubit matrix element is $O(\epsilon)$, and in the low bias regime $\epsilon \ll \Delta$ the off-diagonal component overwhelms the fluctuation in the diagonal part: $|\zeta|/|\xi^{(\pm)}| \ll 1$. In Fig. 1 we depict the real and the imaginary parts of the off-diagonal element of the reduced qubit density matrix. Moreover, as the imaginary part of the off-diagonal matrix element $\xi^{(\pm)}$ is $O(\epsilon)$, in the $\epsilon \ll \Delta$ limit its real part gives the major contribution.

Towards making a quantitative comparison between the closed form expression (3.4) of the density matrix element $\xi^{(+)}$ with the corresponding sum given in (2.14) we use full time-evolution data presented in Fig. 1. For both real and imaginary parts of $\xi^{(+)}$ we compute the magnitudes of their differences between the series evaluation (2.14) and the corresponding theta function based result (3.4). The time-averaged values of these quantities are given by $\langle |\Delta \text{Re}(\xi^{(+)})| \rangle_{\text{av}} = 0.01174$ and $\langle |\Delta \text{Im}(\xi^{(+)})| \rangle_{\text{av}} = 0.00376$, respectively. These objects obtained via series evaluation (2.14) read: $\langle |\text{Re}(\xi^{(+)})| \rangle_{\text{av}} = 0.12149$ and $\langle |\text{Im}(\xi^{(+)})| \rangle_{\text{av}} = 0.0296$. The order of accuracy for the theta function based evaluations in the parametric regime considered here is, therefore, around 90%. The accuracy may be further improved by incorporating higher order terms in the bias parameter ϵ .

The revival and collapse process of $\xi^{(\pm)}$ is evident in Fig. 1. To understand the revival time of the off-diagonal element $\xi^{(\pm)}$ we, for simplicity, study the time dependent terms in (3.4) for the limiting case $\epsilon = 0$ and $x \ll 1$, where the dominant term is $O(\sqrt{x})$. For the range $|\alpha_+| \sim 1.5 - 2$ the structure of the corresponding terms in (3.4) suggests that the oscillation with a *very* short time period (T_{short}) occurs due to the phase $\varphi_{1,0}$, whereas a longer time period (T_{revival}) is generated by the leading phase factor in the theta function. Up to the order of approximation described here these periods read $T_{\text{short}} = \pi((1 - \frac{x}{2})\tilde{\Delta})^{-1}$ and $T_{\text{revival}} = \pi(x\tilde{\Delta})^{-1}$, respectively. For $\alpha = 2$, $\lambda = 0.08\omega$ their numerical values measured in the scaled time read as $T_{\text{short}} = 21.5$ and $T_{\text{revival}} = 828.7$, which show good agreement with the corresponding results (22.9 and 821.6) obtained via (2.14). For a relatively higher coupling strength $\lambda/\omega \lesssim 0.2$ more terms in (3.4) need to be considered to estimate T_{revival} . At a still higher value of λ the picture of revival becomes fuzzy as a large number of modes with incommensurate frequencies produce a phase randomization.

The time evolution of the entanglement of the quasi-Bell initial state (2.9) may be measured by

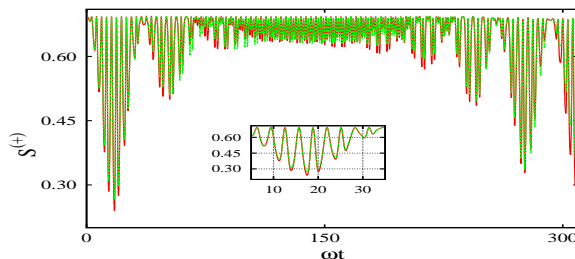


Figure 2: Evaluation of the entropy for $\lambda = 0.15\omega$, $\Delta = 0.15\omega$, $\epsilon = 0.01\omega$ and $\alpha = 2$ using the series (2.13, 2.14) (red solid), and theta function (3.3, 3.4) (green dashed).

the corresponding von Neumann entropy $S^{(\pm)}$. Employing (2.19) and our evaluations (3.3, 3.4) we may find a theta function dependent expression for the time evolution of the entropy in the parametric domain discussed earlier. This may be compared with the expression of the entropy based on the sums (2.19, 2.13, 2.14) as a check on the validity of our closed form evaluation scheme. As these expressions are voluminous, we only reproduce in Fig. 2 the corresponding diagrams for the time evolution of the entropy. Up to the first few revivals for $\xi^{(+)}$ we observe that the entropy obtained via the series sum is well-approximated by the analytical closed form expression. During the revival of the qubit density matrix elements the entropy of the system exhibits drastic fall from its near-maximal value signaling existence of *almost* disentangled pure states of the *subsystems* at corresponding times during their course of evolution. We will discuss in Subsec. V.D. an instance of this phenomenon in detail. The extent of the dip in entropy increases with increase of the bias parameter.

IV The Q -function of the oscillator density matrix

The Husimi Q -function [29] is a quasi-probability distribution on the complex phase space that provides a description of the time evolution of the quantum state of the oscillator. It assumes non-negative values and is normalized to unity on the phase space. For our choice of the quasi-Bell initial states (2.9) it is defined as the expectation value of the reduced density matrix of the oscillator (2.21) in an arbitrary coherent state:

$$Q^{(\pm)}(\beta) = \frac{1}{\pi} \langle \beta | \rho_{\mathcal{O}}^{(\pm)}(t) | \beta \rangle. \quad (4.1)$$

For the state under consideration its explicit positive definite form reads

$$Q^{(\pm)}(\beta) = \frac{1}{2\pi} \exp(-|\alpha_+|^2) \left(\exp(-|\beta_+|^2) |X^\pm|^2 + \exp(-|\beta_-|^2) |Y^\pm|^2 \right), \quad (4.2)$$

where the Fourier sums are given by

$$X^\pm = \sum_{n=0}^{\infty} \frac{(\alpha_+ \beta_+^*)^n}{n!} C_n^\pm(t) \exp(-in\omega t), \quad Y^\pm = \sum_{n=0}^{\infty} (-1)^n \frac{(\alpha_+ \beta_-^*)^n}{n!} C_n^\mp(t)^* \exp(-in\omega t). \quad (4.3)$$

In (4.2, 4.3) we have abbreviated: $\beta_+ = \beta + \lambda/\omega$ and $\beta_- = \beta - \lambda/\omega$. The Q -distribution (4.2) of the reduced density matrix (2.21) does not have any zero on the phase space except at asymptotically large radial distances. The Q -function (4.2) satisfies the normalization condition: $\int Q^{(\pm)}(\beta) d^2\beta = 1$. For later use we note that, in the $\epsilon = 0$ case, the coefficients (2.17) enforce the parity constraint:

$$Q^{(\pm)}(-\beta)|_{\epsilon=0} = Q^{(\pm)}(\beta)|_{\epsilon=0}. \quad (4.4)$$

To study the phase space Q -distribution (4.2) we consider its time-evolution for both the strong (Fig. 3) and the ultra-strong coupling regime. We distinguish between two cases: (i) For the strong

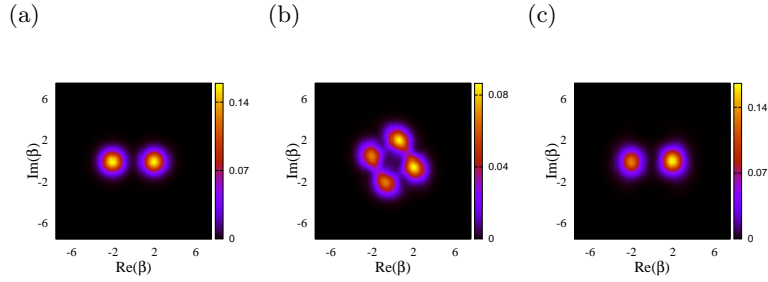


Figure 3: The $Q^{(+)}(\beta)$ function using (4.3) for $\Delta = 0.15\omega$, $\epsilon = 0.01\omega$ and $\alpha = 2$ at various values of scaled time (a) 0, (b) 155 and (c) 300 in the strong coupling domain: $\lambda = 0.15\omega$.

coupling regime where, say, the parametric values described following (3.4) hold, the Laguerre polynomials may be approximated by their quadratic parts. The off-diagonal element in the Hamiltonian (2.6) then contains effective interaction terms up to $O(x^2\tilde{\Delta})$. In the *short-term time scale* $t \ll (x^2\tilde{\Delta})^{-1}$ observed in Fig. 3 the corresponding $Q^{(+)}(\beta)$ function exhibits a quasi-periodic behavior indicating that an interference pattern develops between the harmonics of the interaction-dependent mode with frequency $O(x\tilde{\Delta})$. This produces pronounced standing waves for some time interval causing bifurcation of each one of the twin quasi-probability peaks, and consequent spreading of the $Q^{(+)}(\beta)$ distribution in the phase space. Signifying a to and fro transfer of energy between the qubit and the oscillator, the periodic splitting and rejoining of the peaks of the Q -distribution correspond, respectively, to the collapse and the revival of the qubit off-diagonal element $\text{Re}(\xi^{(+)})$ (2.14). The physical process is reminiscent of an LC circuit. The time interval (T_{split}) is roughly half of the revival time observed for $\text{Re}(\xi^{(+)})$: $T_{\text{split}} \cong T_{\text{revival}}/2$. This can be readily inferred from Figs. 1 (a) and 3 (b). Interaction modes of frequency $O(x^2\tilde{\Delta})$ generate quasi-periodic behavior in a *very long time scale*. This will be discussed in detail in Subsec. V.A. In the presence of a Kerr-type of nonlinear Hamiltonian an initial coherent state is known to evolve [30-33], at specified times, to discrete superposition of coherent states. We will discuss the similarities and dissimilarities of these results with that of the present example in Subsec. V.B. (ii) For the ultra-strong coupling domain $\lambda \sim \omega$ interaction modes with frequencies $\{O(x^n\tilde{\Delta})|n = 0, 1, \dots\}$ and their harmonics rapidly develop and produce a fully randomized interference pattern. The randomness of the phases of the oscillator interaction modes erases any extant phase relation between the ground state and the excited state of the atomic two level system. This causes disappearance of the collapse and revival properties of the atomic density matrix elements. The Q -distribution in the phase space now occupies a wider area and exhibits a chaotic evolution pattern without returning to its initial configuration within a finite time. We will discuss these issues in Sec. V.

One of the utilities of the Q -distribution is that it provides a convenient evaluation of the expectation values of the operators expressed in their antinormal ordered form. The first and second moments of the quadrature variable defined as

$$X_\theta = \frac{1}{\sqrt{2}}(ae^{-i\theta} + a^\dagger e^{i\theta}) \quad (4.5)$$

may be expressed [29] via the following phase space integrals over the complex plane:

$$\begin{aligned} \langle X_\theta \rangle^{(\pm)} &\equiv \text{Tr}(X_\theta(a, a^\dagger)\rho_{\mathcal{O}}^{(\pm)}(t)) = \frac{1}{\sqrt{2}} \int (\beta e^{-i\theta} + \beta^* e^{i\theta}) Q^{(\pm)}(\beta) d^2\beta, \\ \langle X_\theta^2 \rangle^{(\pm)} &\equiv \text{Tr}(X_\theta^2(a, a^\dagger)\rho_{\mathcal{O}}^{(\pm)}(t)) = \frac{1}{2} \int \left((\beta e^{-i\theta} + \beta^* e^{i\theta})^2 - 1 \right) Q^{(\pm)}(\beta) d^2\beta. \end{aligned} \quad (4.6)$$

Employing the Fourier sum (4.2) and using the following notations for the coefficients

$$\begin{aligned} G_{n;\ell}^{\pm}(\theta;t) &= \alpha_+^{\ell} \left(C_{n+\ell}^{\pm}(t) C_n^{\pm}(t)^* + C_{n+\ell}^{\mp}(t)^* C_n^{\mp}(t) \right) \exp(-i\ell(\omega t + \theta)), \\ \mathcal{G}_{n;\ell}^{\pm}(\theta;t) &= \alpha_+^{\ell} \left(C_{n+\ell}^{\pm}(t) C_n^{\pm}(t)^* - C_{n+\ell}^{\mp}(t)^* C_n^{\mp}(t) \right) \exp(-i\ell(\omega t + \theta)), \end{aligned} \quad (4.7)$$

the first two moments of the quadrature are enlisted as a sum on the modes:

$$\langle X_{\theta} \rangle^{(\pm)} = \frac{1}{\sqrt{2}} \exp(-|\alpha_+|^2) \sum_{n=0}^{\infty} \frac{|\alpha_+|^{2n}}{n!} \operatorname{Re} \left(\mathcal{G}_{n;1}^{\pm}(\theta;t) \right) \pm \sqrt{2x} \cos \theta \zeta, \quad (4.8)$$

$$\begin{aligned} \langle X_{\theta}^2 \rangle^{(\pm)} &= |\alpha_+|^2 + \frac{1}{2} \left(1 + x \cos^2 \theta + \exp(-|\alpha_+|^2) \sum_{n=0}^{\infty} \frac{|\alpha_+|^{2n}}{n!} \times \right. \\ &\quad \left. \times \operatorname{Re} \left(G_{n;2}^{\pm}(\theta;t) - 2\sqrt{x} G_{n;1}^{\pm}(\theta;t) \cos \theta \right) \right). \end{aligned} \quad (4.9)$$

The variance of the quadrature reads: $V_{\theta} = \langle X_{\theta}^2 \rangle - \langle X_{\theta} \rangle^2$, which we will later employ for studying emergence of the squeezed state during time evolution. For later utilization we also quote here the mean photon number $\langle \hat{n} \rangle^{(\pm)} = \operatorname{Tr}(a^{\dagger} a \rho_{\mathcal{O}}^{(\pm)}(t))$ and its variance $\langle \Delta \hat{n}^2 \rangle^{(\pm)} = \operatorname{Tr}(\hat{n}^2 \rho_{\mathcal{O}}^{(\pm)}(t)) - (\langle \hat{n} \rangle^{(\pm)})^2$:

$$\langle \hat{n} \rangle^{(\pm)} = |\alpha_+|^2 + \frac{\lambda^2}{\omega^2} - \frac{\lambda}{\omega} \exp(-|\alpha_+|^2) \sum_{n=0}^{\infty} \frac{|\alpha_+|^{2n}}{n!} \operatorname{Re}(G_{n;1}^{\pm}(t)), \quad (4.10)$$

$$\begin{aligned} \langle \Delta \hat{n}^2 \rangle^{(\pm)} &= |\alpha_+|^2 + \frac{\lambda^2}{\omega^2} (1 + 2|\alpha_+|^2) - \frac{\lambda}{\omega} \exp(-|\alpha_+|^2) \sum_{n=0}^{\infty} \frac{|\alpha_+|^{2n}}{n!} \times \\ &\quad \times (1 + 2n - 2|\alpha_+|^2) \operatorname{Re}(G_{n;1}^{\pm}(t)) - \frac{\lambda^2}{\omega^2} \exp(-2|\alpha_+|^2) \times \\ &\quad \times \left[\sum_{n=0}^{\infty} \frac{|\alpha_+|^{2n}}{n!} \operatorname{Re}(G_{n;1}^{\pm}(t)) \right]^2 + \frac{\lambda^2}{\omega^2} \exp(-|\alpha_+|^2) \sum_{n=0}^{\infty} \frac{|\alpha_+|^{2n}}{n!} \operatorname{Re}(G_{n;2}^{\pm}(t)). \end{aligned} \quad (4.11)$$

Using the procedure developed in Sec. III and the Q -function (4.2), an arbitrary moment of the oscillator dynamical variables may be obtained as linear combinations of the Jacobi theta functions. We now demonstrate this for the first two moments of the quadrature variable (4.8, 4.9). To this end we retain up to the quadratic terms in the expansion of the Laguerre polynomials and maintain the range of parameters described following (3.4). The first moment of the quadrature is non-vanishing only in the presence of a bias term ($\epsilon \neq 0$) in the qubit Hamiltonian (2.1):

$$\langle X_{\theta} \rangle^{(\pm)} = \frac{\epsilon}{\tilde{\Delta}} \frac{\exp(-|\alpha_+|^2/2)}{\sqrt{4\pi|\alpha_+|^2}} \left(\mathcal{I}_1^{\theta} \operatorname{Im}(\mathbb{T}) \pm \mathcal{R}_1^{\theta} \operatorname{Re}(\mathbb{H}) \right) \pm \sqrt{2x} \cos \theta \zeta, \quad (4.12)$$

where the linear combinations of the Jacobi theta functions read, respectively, as

$$\begin{aligned} \mathbb{T} &= \left((2 + x + x^2) \sqrt{\tilde{\varphi}_0} + \left(2 + \frac{7x}{2} \right) f \sqrt{\tilde{\varphi}_2} + \frac{3}{2} f^2 \sqrt{\tilde{\varphi}_4} \right) \vartheta_3(\mathbf{q}, \mathfrak{z}_1) \\ &\quad + x(1+x) \varphi_{1,0} \vartheta_3(q, z_1) + \frac{3}{2} x f \varphi_{3,1} \vartheta_3(q, z_3), \\ \mathbb{H} &= \left(x(1+x) \sqrt{\tilde{\varphi}_0} - \frac{3}{2} x f \sqrt{\tilde{\varphi}_2} \right) \vartheta_4(\mathbf{q}, \mathfrak{z}_1) \\ &\quad - x(1+x) \varphi_{1,0} \vartheta_4(q, z_1) + \frac{3}{2} x f \varphi_{3,1} \vartheta_4(q, z_3), \end{aligned} \quad (4.13)$$

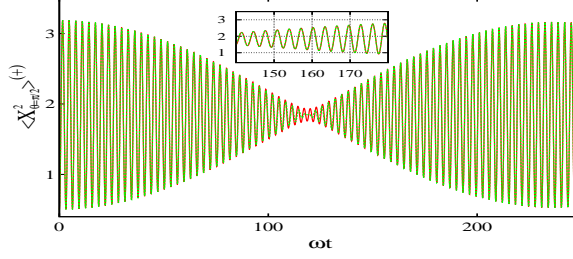


Figure 4: The evaluation of the second moment of the quadrature variable $\langle X_{\pi/2}^2 \rangle^{(+)}$ for the values $\lambda = 0.16\omega$, $\Delta = 0.15\omega$, $\epsilon = 0.01\omega$ and $\alpha = 1$ using the series (4.9) (red solid), and theta function (4.14) (green dashed).

and $\mathcal{R}_n^\theta = \text{Re}(\tilde{\alpha}^{(n)} \exp(-in\theta))$, $\mathcal{I}_n^\theta = \text{Im}(\tilde{\alpha}^{(n)} \exp(-in\theta))$. Similarly, the second moments of the quadrature may also be expressed via the Jacobi theta functions as follows:

$$\begin{aligned} \langle X_\theta^2 \rangle^{(\pm)} &= \frac{1}{2}(1 + x \cos^2 \theta) + |\alpha_+|^2 + \frac{\exp(-|\alpha_+|^2/2)}{\sqrt{2\pi|\alpha_+|^2}} \times \\ &\times \left(\mathcal{R}_2^\theta \text{Re}(\mathcal{T}) \pm \mathcal{I}_2^\theta \text{Im}(\mathcal{H}) - 2\sqrt{x} \cos \theta \left(\mathcal{R}_1^\theta \text{Re}(\mathbf{T}) \mp \mathcal{I}_1^\theta \text{Im}(\mathbf{H}) \right) \right), \end{aligned} \quad (4.14)$$

where the respective linear sums of ϑ_3 and ϑ_4 functions read:

$$\begin{aligned} \mathcal{T} &= \left(1 - \frac{\epsilon^2 x^2}{\tilde{\Delta}^2}\right) \tilde{\varphi}_1 \vartheta_3(\mathbf{q}, \mathfrak{z}_2) + \frac{\epsilon^2 x^2}{\tilde{\Delta}^2} \varphi_{2,1} \vartheta_3(q, z_2), \\ \mathcal{H} &= \left[\left(1 - \frac{\epsilon^2}{2\tilde{\Delta}^2} \left(1 + 2x + \frac{11x^2}{2}\right)\right) \tilde{\varphi}_1 + \frac{\epsilon^2}{\tilde{\Delta}^2} f(1 + 4x) \tilde{\varphi}_3 \right. \\ &\quad \left. - \frac{5\epsilon^2}{4\tilde{\Delta}^2} f^2 \tilde{\varphi}_5 \right] \vartheta_4(\mathbf{q}, \mathfrak{z}_2) - \frac{\epsilon^2}{\tilde{\Delta}^2} x \left(1 + \frac{11x}{4}\right) \varphi_{2,1} \vartheta_4(q, z_2) \\ &\quad + \frac{5\epsilon^2}{2\tilde{\Delta}^2} x f \varphi_{4,3} \vartheta_4(q, z_4), \\ \mathbf{T} &= \left(1 - \frac{\epsilon^2}{\tilde{\Delta}}(1 + x)\right) \varphi_{1,0} \vartheta_3(q, z_1) - \frac{2\epsilon^2}{\tilde{\Delta}^2} f \varphi_{3,1} \vartheta_3(q, z_3) \\ &\quad + \frac{\epsilon^2}{\tilde{\Delta}^2} \left((1 + x) \sqrt{\tilde{\varphi}_0} + 2f \sqrt{\tilde{\varphi}_2} \right) \vartheta_3(\mathbf{q}, \mathfrak{z}_1) \\ \mathbf{H} &= \left(1 - \frac{\epsilon^2}{2\tilde{\Delta}}(1 + x)\right) \varphi_{1,0} \vartheta_4(q, z_1) + \frac{\epsilon^2}{\tilde{\Delta}^2} f \varphi_{3,1} \vartheta_4(q, z_3) \\ &\quad - \frac{\epsilon^2}{2\tilde{\Delta}} x \sqrt{\tilde{\varphi}_0} \vartheta_4(\mathbf{q}, \mathfrak{z}_1). \end{aligned} \quad (4.15)$$

This completes our analytical evaluations of the expectation values of antinormally ordered operators in closed forms involving linear combinations of the theta functions. The procedure is valid for the parametric regime described in Sec. III. In Fig. 4 we compare the values of the second moment $\langle X_{\theta=\pi/2}^2 \rangle^{(+)}$ given by the Fourier sum (4.9) and its theta function based analytical evaluation (4.14). For a quantitative comparison we consider the magnitudes of the differences between the series evaluation (4.9) and the corresponding theta function based computation (4.14). Its time-averaged value over the data presented in Fig. 4 is given by $\langle |\Delta X_{\pi/2}^2 \rangle^{(+)} \rangle_{\text{av}} = 0.03886$, whereas the time-averaged series evaluation (4.9) reads: $\langle |X_{\pi/2}^2 \rangle^{(+)} \rangle_{\text{av}} = 1.84296$. The level of accuracy for the theta function based evaluations in the parametric regime considered here is roughly around 98%.

V Delocalization at ultra-high coupling strength

Our objective in this section is to study the phase space behavior of the system in the ultra-strong coupling domain: $\lambda \sim \omega$. Here we *do not* adhere to the parametric restrictions mentioned following (3.4) except for the fact that the *adiabatic limit* $\Delta \ll \omega$ [13] *still holds*. To explore the evolution (4.2) of the phase space density $Q^{(\pm)}(\beta)$ we use a number of tools described below.

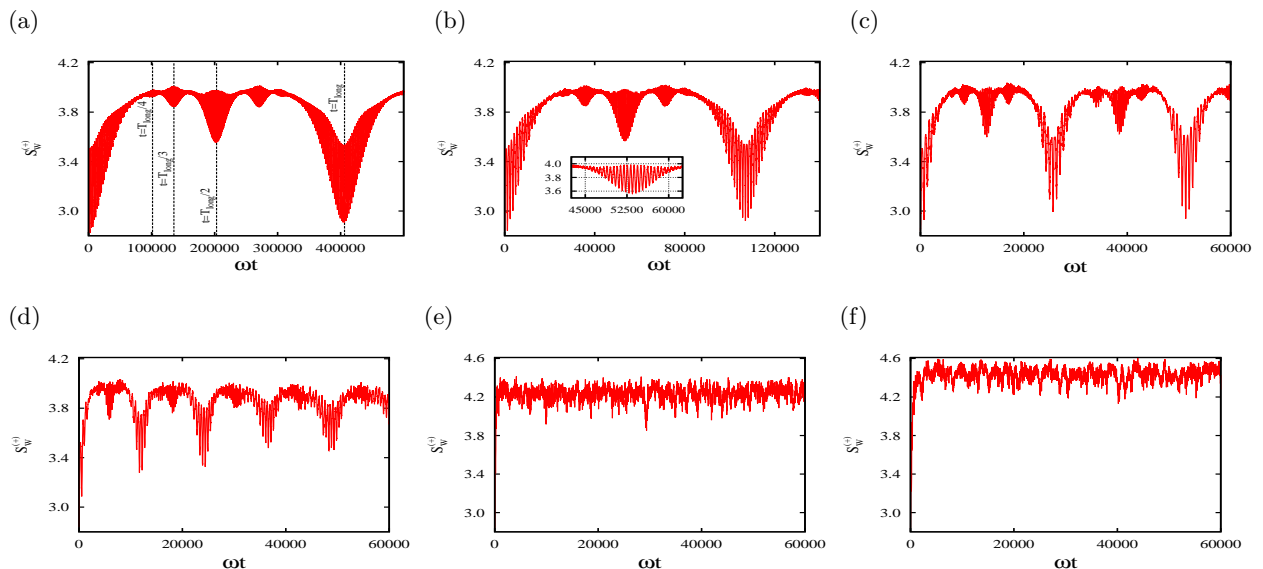


Figure 5: The long time evolution of the Wehrl entropy for $\Delta = 0.15\omega$, $\epsilon = 0.03\omega$ and $\alpha = 3$ at various λ : (a) 0.05ω , (b) 0.07ω (c) 0.1ω , (d) 0.12ω , (e) 0.9ω and (f) 1.3ω .

V.A. Wehrl entropy

The Wehrl entropy [34] defined as

$$S_W^{(\pm)} = - \int Q^{(\pm)}(\beta) \log Q^{(\pm)}(\beta) d^2\beta \quad (5.1)$$

is an information-theoretic measure describing the delocalization of the oscillator in the phase space. It may be regarded [38] as a count of an equivalent number of widely separated coherent states necessary for covering the existing phase-space occupation of the coupled oscillator. It has recently been used for studying quantum phase transitions in several models [39, 40]. In the present case we, using the time evolution (4.2) and the definition (5.1), first numerically study (Fig. 5) the long range time dependence of Wehrl entropy for various values of coupling strength. We observe the following properties: **(i)** We first consider the *long range* $t \gtrsim (x^2 \tilde{\Delta})^{-1}$ quasi-periodicity of the Wehrl entropy evident in Figs. 5 (a, b, c). For the coupling regime ($\lambda \lesssim 0.1\omega$) considered therein the Laguerre polynomials in the effective Hamiltonian (2.6) are well-approximated by their quadratic components. This generates interaction-dependent frequency mode $\sim x^2 \tilde{\Delta}$ and its harmonics. Their interference gives rise to quasi-periodic long time behavior of the coupled oscillator, where the time period satisfies the property $T_{\text{long}} \propto \lambda^{-4} \exp(x/2)$. The time period observed in Figs. 5 (a, b, c) are given in our scale as $T_{\text{long}} = 406081.5$ (for $\lambda = 0.05\omega$), $T_{\text{long}} = 106976.7$ (for $\lambda = 0.07\omega$), $T_{\text{long}} = 25656.6$ (for $\lambda = 0.10\omega$), respectively. The near equality of the quantity $\lambda^4 T_{\text{long}} \exp(-x/2)$ in the respective cases: 2.52535, 2.54346, 2.51486 is a check on the validity of the said truncation of the Laguerre polynomials. This explains the long timespan quasi-periodicity of the system in the coupling regime $\lambda \lesssim 0.1\omega$. We note that a similar behavior in the time-evolution of Wehrl entropy was observed [31] in a Kerr-like

medium. The local minimum in the said evolution diagram [31] corresponded with formation of finite superposition of coherent states. The *long range behavior* (Figs. 5 (a, b, c)) of the Wehrl entropy in the present model qualitatively agrees with the properties obtained in [31]. However, the qubit-oscillator interactions in our case induces undulations of frequency $O(x\tilde{\Delta})$ superposed on the long range oscillations, which now forms an envelop (inset of Fig. 5 (b)) of the total time-evolution of the Wehrl entropy. The physical effects of multiple time scales present in our case will be discussed in Subsec. V.B. **(ii)** We now comment on the initial rate of production of Wehrl entropy in the ultra-strong coupling domain $x \sim 1 \Rightarrow \lambda \gtrsim \omega/2$. With increased qubit-oscillator coupling all high-frequency quantum fluctuation modes are now rapidly generated. Interference among these incommensurate modes cause, in general, quick spread the Q -distribution in the phase space resulting in fast initial production of Wehrl entropy $S_W^{(\pm)}$. The typical time scale for establishing the interference pattern is given, via (2.6), by $T_{\text{ent. prod.}} \tilde{\Delta} L_n(x) \sim 1$. To study the coupling-dependence of initial entropy production time scale $T_{\text{ent. prod.}}$ we note the behavior [41] of the Laguerre function $L_n(x > 0)$ for an asymptotically large value of the index n :

$$L_n(x) = \frac{n^{-\frac{1}{4}} \exp(x/2)}{\sqrt{\pi} x^{\frac{1}{4}}} \cos(2\sqrt{nx} - \pi/4) + O\left(n^{-\frac{3}{4}}\right), \quad (5.2)$$

which immediately produces the estimate $T_{\text{ent. prod.}} \propto \sqrt{\lambda}$. To test the above estimate, we study (Fig. 6) the transient initial production time for $S_W^{(+)}$. Assuming $T_{\text{ent. prod.}} \approx 310$ units for the coupling $\lambda = 0.6\omega$, our asymptotic estimate immediately allows us to predict the said entropy production time for the cases $\lambda = 0.8\omega$ and $\lambda = 1.0\omega$ as 357.96 and 400.21 units, respectively. These predictions are very close to the corresponding numerical values marked in Fig. 6. **(iii)** In the ultra-strong coupling domain $\lambda \sim \omega$ all frequency modes $\{O(x^n\tilde{\Delta})|n = 0, 1, \dots\}$ and their harmonics quickly arise, and due to randomness of their incommensurate phases the resultant interference contributions have a tendency to average out. *After* the period of rapid initial increment ($t \gg T_{\text{ent. prod.}}$), the long time description of the Wehrl entropy given in Figs. 5 (e, f) suggests that high-frequency ($O(\omega)$) quantum fluctuations are superimposed on an almost stationary value. The relative magnitude of the quantum oscillations in the Wehrl entropy remains small: $\left.\frac{|\Delta S_W|}{S_W}\right|_{t \gg T_{\text{ent. prod.}}} \ll 1$. Thus the randomization of the phases of a large number of modes induces an *effective stabilization* of the occupation in the phase space after an initial build-up. The hierarchy of the frequency scales present in our model: $O(\tilde{\Delta}) \ll \omega$ suggests a natural approach towards making the said quasi-stationary property more evident. We qualitatively describe it below. Following [42] we may obtain physically observed quantities after a suitable coarse graining of the time scale that acts as a low-pass filter effectively eliminating the high frequency components in quantum oscillations. The long time behavior of physical quantities, say $S_W^{(+)}$, is set by the interaction modes typically having frequencies $O(\tilde{\Delta})$, while the high oscillator frequency ω gives rise to the rapid fluctuations. A coarse graining *à la* [42] has a smearing effect on the high frequency fluctuations as the implicit time-averaging process described therein has a suitable resolution time $(\tilde{\Delta})^{-1} \gg T_{\text{graining}}^{\text{coarse}} \gg \omega^{-1}$. The contrast between the long time evolution in the strong coupling (Fig. 5 (a, b, c)) and the ultra-strong coupling (Figs. 5 (e, f)) regimes may be stated as follows. In the former case the system undergoes an almost periodic dynamical evolution, while in the latter case the initial state does not recur within a long span of time wherein a quasi-stationary state prevails. This points towards the emergence of a statistical equilibrium. The changeover between the two regimes is evident in Fig. 5 (d). Another significant fact in Fig. 5 is that for a fixed value of the phase-space separation α and in the $\lambda \sim \omega$ regime, the time-averaged value of the Wehrl entropy gradually *increases* with increasing coupling strength. The averaging is considered *after* the transient period of entropy production is over, and the time scale of averaging is taken to be much *longer* than ω^{-1} . An increasing expectation value of the number operator $\langle \hat{n} \rangle$ due to a stronger qubit-oscillator interaction amounts to a wider spread of the Q -function in the phase space causing an increment in the Wehrl entropy.

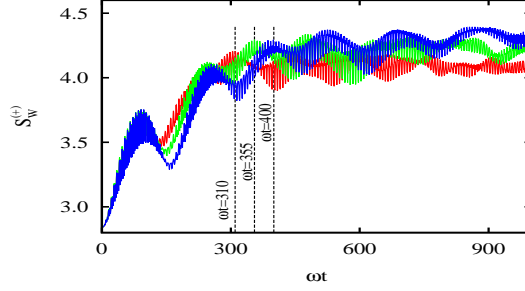


Figure 6: The initial rise of the Wehrl entropy obtained for $\Delta = 0.15\omega$, $\epsilon = 0.03\omega$ and $\alpha = 3$ at various $\lambda = 0.6\omega$ (red), $\lambda = 0.8\omega$ (green) and $\lambda = 1.0\omega$ (blue).

V.B. Kitten states via long and short time oscillations

It is known that in the context of the Kerr-type of nonlinear self-interacting photonic models the local minima in the time evolution of the Wehrl entropy of an initial coherent state are associated [31] with formations of uniformly separated macroscopic superposition of finite number of coherent states [30-33]. These authors noted that these transient superposition of the macroscopic coherent states are realized at rational multiples of the time period of the Q -distribution. The number of distinguishable states participating in the superposition depends linearly on the amplitude of the initial coherent state. Experimental realization of a nonclassical superposition of multiple coherent states in a Kerr medium has been achieved [43] recently. Generation of the cat-like states in an arbitrary finite dimensional bosonic system that admits applying the displacement operation on its ground state has also been studied [44] in a Kerr-type medium.

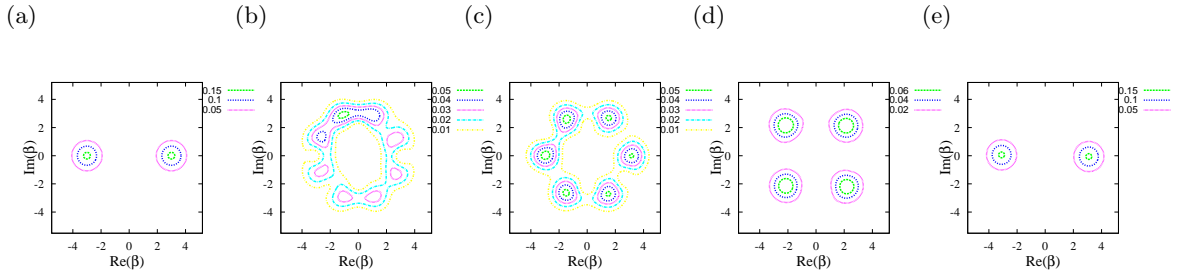


Figure 7: The $Q^{(+)}(\beta)$ function using (4.3) for $\Delta = 0.15\omega$, $\epsilon = 0.03\omega$ and $\alpha = 3$ at various values of scaled time: (a) 0, (b) $T_{\text{long}}/4$, (c) $T_{\text{long}}/3$, (d) $T_{\text{long}}/2$, (e) T_{long} ($= 406081.5$) for the chosen coupling strength $\lambda = 0.05\omega$.

Much parallel to the scenario [30-33] in the Kerr medium, our mixed state Q -distribution (4.2) in the strong coupling limit $\lambda \sim 0.1\omega$ represents momentary realizations of macroscopic coherent states uniformly separated on the phase space at specific times $T_{p,q} = (p/q)T_{\text{long}}$, where (p, q) are coprime integers ($p \leq q$). In the small-bias case the parity symmetry (4.4) of the Q -function (4.2) requires appearance of an *even* number ($2q$) of macroscopically distinguishable Gaussian peaks. This is evident in Fig. 7, where the chosen qubit-oscillator coupling $\lambda = 0.05\omega$ allows the Laguerre polynomials to be approximated by their quadratic components, which produce modes of frequency $\sim x^2 \tilde{\Delta}$ and its harmonics. Starting with the initial quasi-Bell state (2.9) of the composite system, the evolution (Figs. 5 (a) and 7) of the Q -function indicates the transient appearances of 8, 6, 4 uniformly separated Gaussian peaks representing macroscopic coherent states, at rational fractions of the long time quasi-period of the Wehrl entropy: $T_{\text{long}}/4, T_{\text{long}}/3, T_{\text{long}}/2$, respectively. However, the presence of *multiple* time scales due to the qubit-oscillator interaction in the present model introduces another novel interference related feature. As explained in the context of Fig. 3 (b), it follows that in the

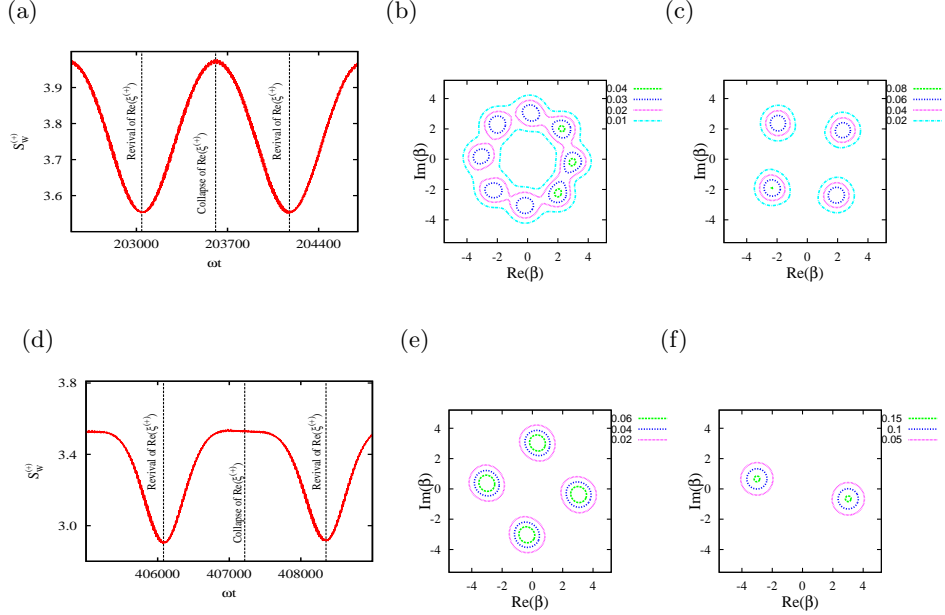


Figure 8: The evolution of Wehrl entropy is given around (a) $T_{\text{long}}/2$ and (d) T_{long} for the coupling strength $\lambda = 0.05\omega$, and $\Delta = 0.15\omega$, $\epsilon = 0.03\omega$ and $\alpha = 3$. Corresponding to the local maxima and minima of the Wehrl entropy the Q -function is given at following scaled times: (b) $T_{\text{long}}/2 + T_{\text{split}}(T_{\text{long}}/2)$, (c) $T_{\text{long}}/2 + 2T_{\text{split}}(T_{\text{long}}/2)$, (e) $T_{\text{long}} + T_{\text{split}}(T_{\text{long}})$, (f) $T_{\text{long}} + 2T_{\text{split}}(T_{\text{long}})$, where $T_{\text{long}} = 406081.5$, $T_{\text{split}}(T_{\text{long}}/2) = 567.5$, $T_{\text{split}}(T_{\text{long}}) = 1135$.

vicinity of time $\{T_{p,q} = (p/q)T_{\text{long}} | (p,q) = 1\}$ interference pattern develops between the harmonics of the interaction-dependent *linear* mode with frequency $O(x\tilde{\Delta})$. This causes an energy transfer in a *short* time scale between the qubit and the oscillator degree of freedom causing a bifurcation (*à la* Fig. 3 (b)) of the $2q$ quasi-probability peaks to $4q$ equally separated Gaussian peaks representing coherent state density matrices. We illustrate this in Fig. 8. The *local* variations of Wehrl entropy in the neighborhood of $(p/q)T_{\text{long}}$ are given in Figs. 8 (a) and (d), where we fix $p = 1; q = 2, 1$, respectively. The Wehrl entropy reaches its local minima at the stipulated times $T_{\text{long}}/2, T_{\text{long}}$. The corresponding ‘kitten’ states with 4 and 2 Gaussian peaks are observed in Figs. 7 (d) and (e), respectively. These regions correspond to the revival of the qubit off-diagonal matrix element $\text{Re}(\xi^{(+)})$ given in (2.14). Doubling of the number of Gaussian peaks to $4q$, as it is manifest in Figs. 8 (b) and (e), occurs at $(1/q)T_{\text{long}} + T_{\text{split}}(T_{\text{long}}/q)$ ($q = 2, 1$, respectively) coinciding with the *collapse* of the element $\text{Re}(\xi^{(+)})$ that leads to local *maximization* of the Wehrl entropy. At subsequent revival of the element $\text{Re}(\xi^{(+)})$ at $(1/q)T_{\text{long}} + 2T_{\text{split}}(T_{\text{long}}/q)$ the number of macroscopic Gaussian peaks again reduces to $2q$. Moreover, the short range splitting time at a particular rational fraction $(p/q)T_{\text{long}}$ scales inversely with q . For instance, from Figs. 8 (a) and (d) we observe that $T_{\text{split}}(T_{\text{long}}/2) \approx (1/2)T_{\text{split}}(T_{\text{long}})$. In other words, due to the complex nature of the qubit-oscillator interaction in the strong coupling regime $\lambda \sim 0.1\omega$ the high frequency quantum oscillations $O(x\tilde{\Delta})$ are *frequency modulated* by the low frequency component $O(x^2\tilde{\Delta})$. Lastly, a finite bias ϵ breaks the parity symmetry (4.4) of the Q -function (4.2), which may now evolve into an odd number of Gaussian peaks at suitable times. We will discuss this issue elsewhere.

V.C. Complexity

Towards understanding the approach to ergodicity in the phase space the authors of Ref. [35] introduced another measure of the delocalization that qualitatively reciprocates the Wehrl entropy, which is found to be difficult for analytical computation due to the presence of the logarithmic function in it. They proposed [35] the inverse of the second moment of the Q -distribution as a measure of complexity of the corresponding quantum states:

$$\mathcal{W}_2(Q) = (\mathcal{M}_2(Q))^{-1}, \quad \mathcal{M}_2(Q^{(\pm)}) = \int (Q^{(\pm)}(\beta))^2 d^2\beta. \quad (5.3)$$

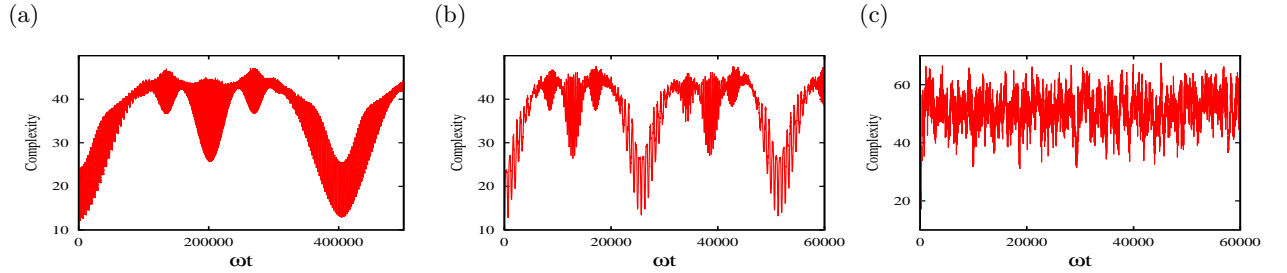


Figure 9: The long time evolution of the complexity $\mathcal{W}_2(Q)$ obtained for $\Delta = 0.15\omega$, $\epsilon = 0.03\omega$ and $\alpha = 3$ at the following values of λ : (a) 0.05ω , (b) 0.1ω and (c) 0.9ω .

The complexity of the quantum state $\mathcal{W}_2(Q)$ represents the effective phase space occupied by the Q -distribution of the oscillator density matrix. The expansion (4.2) allows us to evaluate the second moment of the Q -distribution as follows:

$$\begin{aligned} \mathcal{M}_2(Q^{(\pm)}) &= \frac{1}{8\pi} \exp(-2|\alpha_+|^2) \left(\sum_{N=0}^{\infty} \frac{|\alpha_+|^{2N}}{2^N N!} \mathcal{D}_N(t) + 2 \exp\left(-\frac{x}{2}\right) \sum_{N,M=0}^{\infty} \alpha_+^N (\alpha_+^*)^M \times \right. \\ &\quad \times \exp(-i(N-M)\omega t) \sum_{\mu=0}^{\min(N,M)} \frac{\left(\frac{\lambda}{\omega}\right)^{N+M-2\mu}}{2^\mu \mu! (N-\mu)! (M-\mu)!} \times \\ &\quad \left. \times \mathcal{F}_{N,\mu}^\pm(t) \mathcal{F}_{M,\mu}^\pm(t)^* \right), \end{aligned} \quad (5.4)$$

where the mode sums on the oscillator states are given by

$$\begin{aligned} \mathcal{D}_N(t) &= \left| \sum_{n=0}^N \binom{N}{n} \mathcal{C}_n^+(t) \mathcal{C}_{N-n}^+(t) \right|^2 + \left| \sum_{n=0}^N \binom{N}{n} \mathcal{C}_n^-(t) \mathcal{C}_{N-n}^-(t) \right|^2, \\ \mathcal{F}_{N,\mu}^\pm(t) &= \sum_{n=0}^N \Lambda_{N,n,\mu} \mathcal{C}_n^\pm(t) \mathcal{C}_{N-n}^\mp(t)^*, \quad \Lambda_{N,n,\mu} = \sum_k (-1)^k \binom{\mu}{k} \binom{N-\mu}{N-n-k}. \end{aligned} \quad (5.5)$$

The above expression constitute our analytical evaluation of the complexity measure $\mathcal{W}_2(Q)$. Our plot for the long time behavior of the complexity $\mathcal{W}_2(Q)$ is given in Fig. 9. Agreeing with the assertion in [35], its properties faithfully resemble those of the Wehrl entropy. In Figs. 9 (a, b), where the coupling strength remains $\lambda \lesssim 0.1\omega$, we find that $\mathcal{W}_2(Q)$ exhibits, exactly parallel to the pattern observed for the Wehrl entropy, a quasi-periodic behavior with the time period inversely proportional to $\lambda^4 \exp(-x/2)$. Chaotic character of $\mathcal{W}_2(Q)$ sets in (Fig. 9 (c)) for the ultra-strong coupling regime $\lambda \gtrsim 1.0\omega$. The initial time period of a rapid increase in $\mathcal{W}_2(Q)$ in the vicinity of $\lambda \sim 1.0\omega$ varies as $\sqrt{\lambda}$. We observe in Fig. 9 (c) that, in the ultra-high coupling regime $\lambda \gtrsim \omega$ the complexity $\mathcal{W}_2(Q)$ assumes, mimicking the Wehrl entropy, a quasi-stationary state, except for the high frequency random oscillations that may be eliminated by the coarse graining process.

V.D. Quadrature squeezing and Mandel parameter

For small values of the phase space separation α , quantum interferences manifest in the time evolution of the Q -distribution (4.2) give rise to various features of the nonclassicality such as appearance of squeezed states and negative values of the Mandel parameter. The signature of the squeezing is observed in Fig. 10 at certain times when the variance $V_{\theta=0}^{(+)}$ of the quadrature variable, say at $\theta = 0$, is rendered less than its classical value $\frac{1}{2}$ that holds for the normalization (4.5). For a small separation α in phase space, the states $|\pm\alpha\rangle$ interfere and a contour plot of the Q -distribution (Fig. 10 (c)) makes the quadrature squeezing evident. Beginning with a circular shape (Fig. 10 (b)) the Q -function turns into an ellipse (Fig. 10 (c)) and squeezing appears in an appropriate direction. It follows from Fig. 11 that at the scaled time $\omega t = 408.5$ the quadrature variance reaches a minimum value 0.3741 at an angle $\theta = 5.71^\circ$. The polar angle at which the minimum quadrature variance is realized varies with time and depends on the dynamical state of interference of the quantum modes. An increase in the coupling λ first enhances the squeezing as the quadratic term appearing in the expansion of the Laguerre polynomial in the interaction Hamiltonian (2.6) plays a key role in producing the squeezing, much parallel to that of a Kerr-like interaction [45]. The squeezing is, however, present during part of the oscillations. The coarse-graining process [42] discussed before removes the squeezing property as the measured quantity is averaged over time $T_{\text{graining}}^{\text{coarse}}$. In the ultra-strong coupling regime the squeezing property is eliminated altogether since the phase coherence properties of the Q -distribution, which is necessary for the squeezing to appear, is destroyed in the domain $\lambda \sim \omega$ where the interaction modes $\{O(x^n \tilde{\Delta})|n = 0, 1, \dots\}$ of all orders with incommensurate frequencies arise.

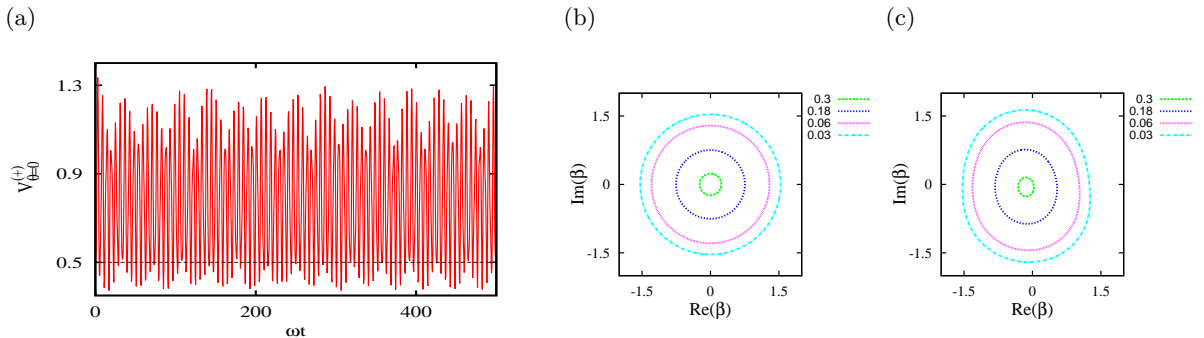


Figure 10: (a) The time evolution of the quadrature variance $V_{\theta=0}^{(+)}$, and the Q function at two different scaled times: (b) 0, and (c) 408.5 for values $\alpha = 0.05$, $\lambda = 0.3\omega$, $\Delta = 0.15\omega$ and $\epsilon = 0.03\omega$. The squeezing at scaled time $\omega t = 408.5$ is evident from the corresponding variance $V_{\theta=0}^{(+)} = 0.3777$. The contour plot (c) also turns elliptic at the said time.

We note that the squeezed state described in Figs. 10 (c), 11 is a *nearly pure state* of the oscillator since, at the particular time, its von Neumann entropy $S^{(+)}|_{\omega t=408.5} = 0.0374$ measuring the mixedness is much lower than the maximal value. This property may also be studied by observing the qubit reduced density matrix. During its time evolution whenever the oscillator reaches a *nearly pure state*, the qubit also evolves *close* to a pure state of its own. For inspection, we construct the corresponding qubit density matrix via (2.12-2.14):

$$\rho_Q^{(+)}(\omega t = 408.5) = \begin{pmatrix} 0.6403 & 0.4703 + i 0.0552 \\ 0.4703 - i 0.0552 & 0.3597 \end{pmatrix}. \quad (5.6)$$

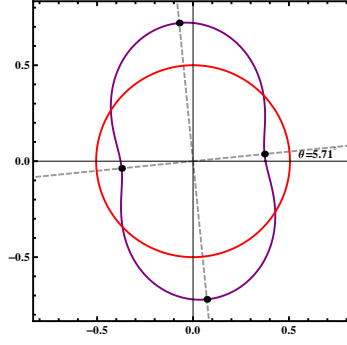


Figure 11: The polar plot (w.r.t θ) of the quadrature variance $V_\theta^{(+)}$ for values $\alpha = 0.05$, $\lambda = 0.3\omega$, $\Delta = 0.15\omega$ and $\epsilon = 0.03\omega$ at time $\omega t = 0$ (red), and $\omega t = 408.5$ (purple) when the least value of variance 0.3741 occurs at an angle $\theta = 5.71^\circ$.

Its eigenvalues and the corresponding eigenvectors read: $\lambda_1 = 0.9939$, $\lambda_2 = 0.0061$, and $|\lambda_1\rangle = (0.7958 + i 0.0935)|1\rangle + 0.5983|-1\rangle$, $|\lambda_2\rangle = (0.5942 + i 0.0698)|1\rangle + 0.8013|-1\rangle$, respectively. We observe that the qubit overwhelmingly (99%) stays at the pure state $|\lambda_1\rangle$. Physically, emergence of a squeezed state requires proper phase correlation between the quantum modes. Occurrence of a random statistical mixture comprising of a large number of pure quantum states destroys the phase correlation. Therefore, the emergence of squeezed states during the time evolution of the composite system is possible when the oscillator (qubit) stays *close* to a pure state.

The Mandel parameter [36] is often used to determine the classical-quantum boundary in experiments where photons are directly detected. It captures any sub-Poissonian behavior in the photon statistics, and acts as a witness to nonclassicality:

$$\mathcal{Q}_M^{(\pm)} \equiv \langle \Delta \hat{n}^2 \rangle^{(\pm)} / \langle \hat{n} \rangle^{(\pm)} - 1. \quad (5.7)$$

The coherent state with $\mathcal{Q}_M = 0$ characterizes the Poissonian statistics and serves as the benchmark for the classical behavior. In the current model the interference between the states $|\pm\alpha\rangle$ for small values of the phase space separation α produces sub-Poissonian photon statistics $\mathcal{Q}_M < 0$ at certain times during part of the oscillatory cycle. Parallel to the emergence of the squeezed states discussed earlier the sub-Poissonian property is aided by an initial increase in the coupling since then only the first few nonlinear interaction terms become prominent. In the ultra-strong coupling domain, however, it is diminished due to the loss of coherence as nonlinear interaction terms of all orders become active.

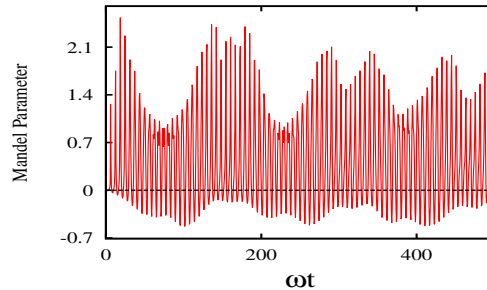


Figure 12: The time evolution of the Mandel parameter for values $\alpha = 0.05$, $\lambda = 0.6\omega$, $\Delta = 0.15\omega$ and $\epsilon = 0.03\omega$.

Moreover, the ultra-strong coupling enhances the expectation value of the number of photonic excitations (4.10). The sub-Poissonian statistics is realized when the number of excitations (4.10) is *not macroscopically large*: $\langle \hat{n} \rangle^{(\pm)} \lesssim 1$. Using the definition (5.7) and the expectation values (4.10),

4.11), we now obtain $\mathcal{Q}_{\mathcal{M}}^{(\pm)} = \mathcal{O}^{(\pm)} / \langle \hat{n} \rangle^{(\pm)}$, where the numerator reads

$$\begin{aligned} \mathcal{O}^{(\pm)} &= \frac{2\lambda^2}{\omega^2} |\alpha_+|^2 - \frac{2\lambda}{\omega} \exp(-|\alpha_+|^2) \sum_{n=0}^{\infty} \frac{|\alpha_+|^{2n}}{n!} (n - |\alpha_+|^2) \text{Re}(G_{n;1}^{\pm}(t)) \\ &+ \frac{\lambda^2}{\omega^2} \exp(-|\alpha_+|^2) \left(\sum_{n=0}^{\infty} \frac{|\alpha_+|^{2n}}{n!} \text{Re}(G_{n;2}^{\pm}) - \exp(-|\alpha_+|^2) \left[\sum_{n=0}^{\infty} \frac{|\alpha_+|^{2n}}{n!} \text{Re}(G_{n;1}^{\pm}) \right]^2 \right). \end{aligned} \quad (5.8)$$

In Fig. 12 we find that at various time segments during the oscillatory cycle the Mandel parameter achieves significantly negative values. Due to the coarse-graining process discussed earlier the quantum interference terms in the Q -function is again suppressed and the negativity of the Mandel parameter disappears. However, the negativity of the Mandel parameter is more robust than the squeezing property against chaotic behavior in the phase space in the ultra-strong coupling domain. Another useful characterization of the nonclassicality of the oscillator density matrix is provided by the Wigner W -distribution [29] that may be determined [46] via a summation procedure involving the matrix elements of the oscillator density matrix (2.21) in the displaced number states. A more complete discussion of the observed negativity in the time evolution of the Wigner W -distribution in the present model will be given elsewhere.

VI Conclusion

Using the adiabatic approximation we investigate a qubit-oscillator bipartite system in the presence of a static bias term in the Hamiltonian for the strong and the ultra-strong coupling regimes. Starting with an entangled quasi-Bell state we obtain the evolution of the reduced density matrices of the qubit and the oscillator. Identifying the series with the Jacobi theta functions in the strong coupling domain we evaluate the qubit density matrix elements in closed form as linear combinations of the theta functions. The phase space Q -distribution is obtained via the oscillator reduced density matrix. The Q -function, in turn, provides closed form expressions of, say, the first two moments of the quadrature variable as linear combinations of the theta functions. The said evaluations of various physical quantities for the strong coupling and weak bias limit are found to be close approximations of their series counterparts which are exact results in the adiabatic scheme. Employing the theta functions, we, in the relevant domain, estimate the revival time of the qubit density matrix and the time of bifurcation of the peaks of the Q -distribution observed in Fig. 3. The differential structure obeyed by the theta functions may also be useful in finding interrelations between various correlation functions appearing in the study of nonclassicality in photon statistics. Moreover, our approach suggests that a suitable generalization of the theta functions may play an important role for the study of the chaotic state in the ultra-strong coupling domain.

For an ultra-high qubit-oscillator coupling strength we study the Wehrl entropy and the complexity $\mathcal{W}_2(Q)$ that measure the delocalization of the oscillator in the phase space. A series expression of the complexity $\mathcal{W}_2(Q)$ is obtained. For the coupling range $\lambda \lesssim 0.1 \omega$ the long-term periodicity is observed to follow from the $O(x^2)$ term in the interaction Hamiltonian. In this regime the Q -distribution corresponding to the initial mixed state density matrix of the oscillator evolves at rational fractions of T_{long} to uniformly separated Gaussian peaks representing ‘kitten’ states. Existence of the interaction-determined multiple time scales in our example, however, gives rise to further bifurcation of Gaussian peaks at times coinciding with the collapse of the off-diagonal qubit density matrix element $\text{Re}(\xi^{(+)})$. In the chaotic $\lambda \sim \omega$ domain the transient production time for the Wehrl entropy has been estimated. Following this period of rapid build up of the Wehrl entropy, the existence of a large number of incommensurate interaction-dependent modes leads to a randomization of the phases and a quasi-stationary behavior sets in. For small values of the phase space amplitude of the quasi-Bell state we observe aspects of the nonclassicality such as existence of *almost* pure squeezed states of the oscillator, and the negativity of the Mandel parameter.

Acknowledgement

We thank R. Chandrashekar for discussions and also for pointing out some references to us. One of us (B.V.J.) acknowledges the support from UGC (India) under the Maulana Azad National Fellowship scheme. We thank a referee for making useful suggestions.

References

- [1] E.T. Jaynes, F.W. Cummings, Proc. IEEE **51**, 89 (1963).
- [2] A.D.Armour, M.P. Blencowe, K.C. Schwab, Phys. Rev. Lett. **88**, 148301 (2002).
- [3] A.A. Anappara, S.D. Liberato, A. Tredicucci, C. Ciuti, G. Biasiol, L. Sorba, F. Beltram, Phys. Rev. B **79**, 201303 (2009).
- [4] T. Niemczyk, F. Deppe, H. Huebl, E.P. Menzel, F. Hocke, M.J. Schwarz, J.J. Garcia-Ripoll, D. Zueco, T. Hümmer, E. Solano, A. Marx, R. Gross, Nature Physics **6**, 772 (2010).
- [5] J.Q. You, F. Nori, Phys. Today **58**, 42 (2005).
- [6] J.Q. You, F. Nori, Nature **474**, 589 (2011).
- [7] P.D. Nation, J.R. Johansson, M.P. Blencowe, F. Nori, Rev. Mod. Phys. **84**, 1 (2012).
- [8] I. Buluta, S. Ashhab, F. Nori, Rep. Prog. Phys. **74**, 104401 (2011).
- [9] I. Buluta, F. Nori, Science, **326**, 108 (2009).
- [10] I.M. Georgescu, S. Ashhab, F. Nori, Rev. Mod. Phys. **86**, 153 (2014).
- [11] Z.L. Ziang, S. Ashhab, J.Q. You, F. Nori, Rev. Mod. Phys. **85**, 623 (2013).
- [12] E.K. Irish, J. Gea-Banacloche, J. Martin, K.C. Schwab, Phys. Rev. B **72**, 195410 (2005).
- [13] S. Ashhab, F. Nori, Phys. Rev. A **81**, 042311 (2010).
- [14] S. Agarwal, S.M. Hashemi Rafsanjani, J.H. Eberly, Phys. Rev. A **85**, 043815 (2012).
- [15] G.E. Andrews, R. Askey, R. Roy, *Special Functions*, Cambridge University Press, Cambridge (1999).
- [16] J. Hausinger, M. Grifoni, Phys. Rev. A **82**, 062320 (2010).
- [17] S.N. Shevchenko, S. Ashhab, F. Nori, Phys. Rep. **492**, 1 (2010).
- [18] S.W. Lee, H. Jeong, Phys. Rev. A **87**, 022326 (2013).
- [19] P. van Loock, W.J. Munro, K. Nemoto, T.P. Spiller, T.D. Ladd, S.L. Braunstein, G.J. Milburn, Phys. Rev. A **78**, 022303 (2008).
- [20] J. Park, H. Saunders, Y. Shin, K. An, H. Jeong, Phys. Rev. A **85**, 022120 (2012).
- [21] Y.X. Liu, L.F. Wei, F. Nori, Phys. Rev. A **71**, 063820 (2005).
- [22] U.L. Anderson, J.S. Neergaard-Nielsen, P. van Loock, A. Furusawa, *Hybrid quantum information processing*, arXiv:1409.37 [quant-ph] (2014).

- [23] H. Jeong, S. Zavatta, M. Kang, S.W. Lee, L.S Costanzo, S. Grandi, T.C. Ralph, M. Bellini, *Nature Photonics* **8**, 564 (2014).
- [24] O. Morin, K. Huang, J. Liu, H. Le Jeannie, C. Fabre, J. Laurat, *Nature Photonics* **8**, 570 (2014).
- [25] Y.X. Liu, L.F. Wei, F. Nori, *Europhys. Lett.* **67**, 941 (2004).
- [26] L.F. Wei, Y.X. Liu, M.J. Storcz, F. Nori, *Phys. Rev. A* **73**, 052307 (2006).
- [27] M. Hofheinz, E.M. Weig, M. Ansmann, R.C. Bialczak, E. Lucero, M. Neeley, A.D. O’Connell, H. Wang, J.M. Martinis, A.N. Cleland, *Nature* **454**, 310 (2008).
- [28] M. Hofheinz, H. Wang, M. Ansmann, R.C. Bialczak, E. Lucero, M. Neeley, A.D. O’Connell, D. Sank, J. Wenner J.M. Martinis, A.N. Cleland, *Nature* **459**, 546 (2009).
- [29] Wolfgang P. Schleich, *Quantum Optics in Phase Space*, Wiley-VCH, Berlin(2001).
- [30] A. Miranowicz, R. Tanaš, S. Kielich, *Quant. Opt.* **2**, 253 (1990).
- [31] I. Jex, A. Orłowski, *J. Mod. Phys.* **41**, 2301 (1994).
- [32] R. Tanas, T. Gantsog, A. Miranowicz, S. Kielich, *J. Opt. Soc. Am. B* **8**, 1576 (1991).
- [33] A. Miranowicz, J. Bajer, M.R.B. Wahiddin, N. Imoto, *J. Phys. A* **34**, 3887 (2001).
- [34] A. Wehrl, *Rev. Mod. Phys.* **50**, 221 (1978).
- [35] A. Sugita, H. Aiba, *Phys. Rev. E* **65**, 036205 (2002).
- [36] L. Mandel, *Opt. Lett.* **4**, 205 (1979).
- [37] H. Araki, E.H. Lieb, *Comm. Math. Phys.* **18**, 160 (1970).
- [38] V. Buzek, C.H. Keitel, P.L. Knight, *Phys. Rev. A* **51**, 2594 (1995).
- [39] E. Romera, R. del Real, M. Calixto, *Phys. Rev. A* **85**, 053831 (2012).
- [40] M. Calixto, R. del Real, E. Romera, *Phys. Rev. A* **86**, 032508 (2012).
- [41] D. Borwein, J. M. Borwein, R. E. Crandall, *SIAM J. Numer. Anal.* **46**, 3285 (2008).
- [42] D.F.V. James, J. Jerke, *Can. J. Phys.* **85**, 625 (2007).
- [43] G. Kirchmair, B. Vlastakis, Z. Leghtas, S.E. Nigg, H. Paik, E. Ginossar, M. Mirrahimi, L. Frunzio, S.M. Girvin, R.J. Schoelkopf, *Nature* **495**, 205 (2013).
- [44] A. Miranowicz, M. Paprzycka, A. Pathak, F. Nori, *Phys. Rev. A* **89**, 033812 (2014).
- [45] R. Tanaš, A. Miranowicz, and S. Kielich, *Phys. Rev. A* **43**, 4014 (1991).
- [46] H. Moya Cessa, P.L. Knight, *Phys. Rev. A* **48**, 2479 (1993).